DIGITAL SIMULATION OF ASSOCIATED AND NONASSOCIATED LIQUID MEMBRANE ELECTROCHEMICAL PROPERTIES

FREDERICK S. STOVER *and* RICHARD P. BUCK

From the William Rand Kenan Laboratories of Chemistry, University of North Carolina, Chapel Hill, North Carolina 27514

ABSTRACT The method and results of a digital simulation of electrochemical properties for associated and nonassociated liquid ion-exchange membranes are presented. It is assumed that the membrane is ideally permselective, sites are completely trapped, electroneutrality holds everywhere in the membrane, and the bathing solutions contain no more than two counterions, of which one is completely dissociated in the membrane. Electrochemical properties are simulated for the single counterion case and in the interference region. Concentration profiles, potentiometric responses, transient potential responses to activity steps, and current-voltage curves are given and the effects of ion-pairing and species mobilities are studied. It is found that ion-pairing increases the potentiometric selectivity toward the complexing ion over the noncomplexing ion. Transient responses to an ion activity step are shown to depend in a complex way on the ion-pair formation constant and the various mobilities. Current-voltage curves are simulated for varying degrees of ion-pairing and qualitative agreement is found with previous theoretical treatments, as well aa quantitative agreement in those cases where closed-form expressions are known.

INTRODUCTION

Modeling electrochemical properties of ideal liquid ion-exchanger membranes is important because of relevance in interpreting responses of ion-selective electrodes. Also, detailed knowledge of passive ion-exchanger ion transport properties may allow precise comparison with corresponding properties of biological membranes. While the applications of these membranes have been extensively studied, (1–3) theoretical descriptions of these systems have lagged behind. Conti and Eisenman (4) first described in detail the steady-state behavior of membranes containing mobile sites with completely dissociated ion pairs. Later, Sandblom et al. (5, 6) extended this theory to include effects of association of the site and counterions to form ion pairs. Because of mathematical complexities introduced therein, explicit solutions were obtained only for a few limiting cases. Sandblom has also treated current-voltage characteristics of strongly associated membranes (7). Buck and Sandifer (8) extended the Conti and Eisenman treatment to include permeable counter-ions of different charge. However, full characterization of liquid membrane electrochemical phenomena has yet to be given, particularly for cases of general association. Direct analysis of the time re-

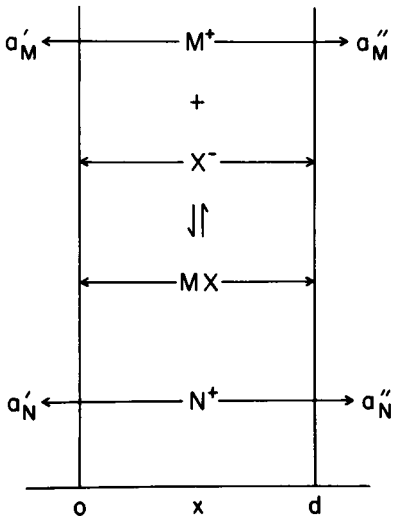

FIGURE 1

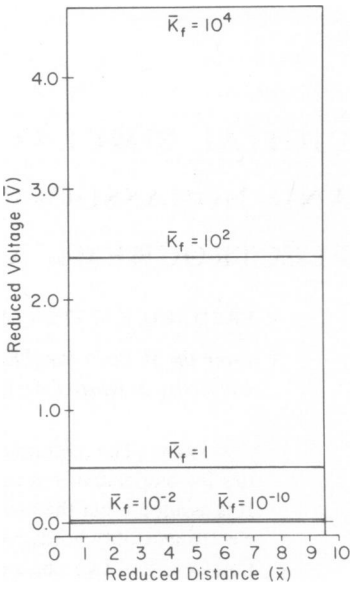

FIGURE 2

FIGURE 1 System of completely trapped mobile sites, X^-, permeable counter ions M^+ and N^+, with ion association between M^+ and X^-.

FIGURE 2 Voltage profiles across electroneutral liquid ion exchanger membranes with a single cation M^+ in the bathing solutions on both sides. Membrane contains M^+ and trapped sites X^- with ion association according to Eq. 2. $a'_M = a''_M = 1$, $\bar{C}^*_X = 1$.

sponses of potential, field, and concentration profiles under electric excitation and activity steps has not been given. However, some information can be inferred from the time constant calculations of Macdonald (9, 10).

It is likely that complete analytical treatments of electrochemical properties at all times for liquid ion-exchanger membranes cannot be given because of the nonlinearity of the Nernst-Planck transport equations. We have therefore turned to the powerful techniques of digital simulation to circumvent the difficulties of direct mathematical analysis of the problems. Digital simulation methods as outlined by Feldberg (11) have been successfully applied to the solution of various electrochemical problems. Sandifer and Buck (12) have demonstrated improvements in Feldberg's algorithm which increase accuracy and decrease computation time. Cohen and Cooley (13) have used digital simulation to find the numerical solution to the time-dependent Nernst-Planck equations for liquid junctions and thin membranes. Sandifer and Buck (14) presented an extension of the Cohen-Cooley technique to include space charge in the membrane via Poisson's equation. Their technique, like that used in this work, is an explicit method. In this work, we apply digital techniques to investigate the electrical properties of a liquid ion-exchange membrane with particular attention being paid to the factors which affect membrane selectivity.

SYSTEM AND MODEL

The system under study, shown in Fig. 1, consists of a membrane phase containing a univalent ion X^-, which acts as a mobile site and is completely trapped within the membrane. The membrane is ideally permselective to cations, i.e. there is total exclusion of co-ions. In addition, there are two univalent counterions, M^+ and N^+, of which N^+ is completely dissociated within the membrane while M^+ may associate with the site to any degree, according to

$$M^+ + X^- \rightleftharpoons MX. \tag{1}$$

Local chemical equilibrium is maintained such that

$$K_f = C_{MX}/(C_M{}^+)(C_X{}^-), \tag{2}$$

and electroneutrality is assumed everywhere in the membrane,

$$C_M{}^+ + C_N{}^+ = C_X{}^-. \tag{3}$$

Also, concentrations of the counterions at membrane boundaries are in a fixed ratio through the Donnan equilibria

$$\frac{C_M{}^+(0 \text{ or } d)}{C_N{}^+(0 \text{ or } d)} = \frac{k_M a_M(' \text{ or } '')}{k_N a_N(' \text{ or } '')}, \tag{4}$$

where k_M and k_N are the partial ion-exchange constants or single-ion partition coefficients (15). Double primes apply to the right-hand or reference side while single primes apply to the left-hand "0" sides. Finally, the boundary condition for sites, because of complete trapping is

$$\frac{1}{d}\int_0^d (C_X{}^- + C_{MX})\,dx = C_X^*, \tag{5}$$

where C_X^* is a constant average concentration at all times. Activity coefficients are taken to be unity.

SIMULATION TECHNIQUE

The digital simulation technique used here is similar to that of Feldberg (11), Cohen and Cooley (13), and Buck and Sandifer (8). Time and distance are discretized into intervals so that concentration derivatives may be approximated by finite differences. Distance intervals are called "volume elements" and are denoted by the subscript j. Following Sandifer, the interfaces of the membranes are placed in the middle of the first and last volume elements so that

$$d = (\text{NVE} - 1)\delta. \tag{6}$$

where d is the total membrane thickness, NVE is the number of volume elements in the membrane, and δ is the thickness of one volume element. Concentrations are

known in the middle of each volume element and the electric fields are known at the volume element interfaces.

Fluxes of each species are given by a Nernst-Planck equation

$$J_{i,j} = -u_i RT(\mathrm{d}C_{i,j}/\mathrm{d}x) + z_i C_{i,j} F E_j, \tag{7}$$

where $J_{i,j}$ and $C_{i,j}$ are the flux and concentration, respectively, of species i in the jth volume element; u_i is its mobility, z_i its charge, and E_j the electric intensity at the volume element interface between j and $j + 1$.

Current density throughout the membrane is given by the faradaic current and the double-layer charging (displacement) current

$$I = \sum_i F J_{i,j} z_i + \epsilon(\mathrm{d}E_j/\mathrm{d}t). \tag{8}$$

In our simulation, however, we take $\epsilon = 0$ to force electroneutrality throughout the membrane. This condition also eliminates from the simulation any short time electrical properties of the membrane due to interfacial charging and leaves for the current density expression only

$$I = \sum_i F J_{i,j} z_i. \tag{9}$$

It is clear from the form of Poisson's equation

$$\epsilon(\mathrm{d}E_j/\mathrm{d}x) = \sum_i z_i C_{i,j} = 0, \tag{10}$$

that this procedure places no special restrictions on the terms $\mathrm{d}E_j/\mathrm{d}t$ and $\mathrm{d}E_j/\mathrm{d}x$, and that Poisson's equation remains coupled to diffusion. The effect of setting $\epsilon = 0$ is elimination of fields due to space charge inside the membrane by collapsing the diffuse layers into the interfaces where they are accounted for in the interfacial potential calculation. Time dependence of species' concentrations are calculated from Fick's second law

$$\partial C_{i,j}/\partial t = -\partial J_{i,j}/\partial x. \tag{11}$$

To simulate membrane responses in a general way, the variables in the equation above are reduced to dimensionless quantities from the relations:

$$\bar{J}_{i,j} = J_{i,j}\delta/u_o C_o RT; \tag{12}$$

$$\bar{x} = x/\delta; \tag{13}$$

$$\bar{E}_j = E_j \delta F/RT; \tag{14}$$

$$\bar{u}_i = u_i/u_o; \tag{15}$$

$$\bar{C}_{i,j} = C_{i,j}/C_o; \tag{16}$$

$$\bar{V} = VF/RT; \tag{17}$$

$$\bar{I} = I\delta/u_o C_o FRT; \tag{18}$$

$$\bar{t} = tu_o RT/\delta^2. \tag{19}$$

Symbols with bars represent dimensionless quantities. V is the potential across the membrane (including interfaces) and it is a function of time. u_o and C_o are the scaling mobility and concentration, F is the Faraday constant, R is the gas constant, and T is the absolute temperature. Using these reduced parameters, Eqs. 7, 9, and 11 may be rewritten in their reduced, finite difference form.

$$\bar{J}_{i,j} = (-\bar{u}_i \Delta \bar{C}_{i,j}/\Delta \bar{x}) + z_i \bar{u}_i \bar{C}_{i,j} \bar{E}'_j, \tag{20}$$

$$\bar{I} = \sum_i z_i \bar{J}_{i,j}, \tag{21}$$

$$\Delta \bar{C}_{i,j}/\Delta \bar{t} = -(\Delta \bar{J}_{i,j}/\Delta \bar{x}), \tag{22}$$

where the flux equation (Eq. 20) is written in terms of a new field, $\bar{E}'_j(t) = \bar{E}_j(t + 1)$; i.e. Eq. 20 is implicit in field.

Distance is normalized by the thickness of a volume element and time is normalized by the diffusion time for a volume element. The result gives $\Delta \bar{x} = 1$ in Eqs. 20 and 22 and $\Delta \bar{t} = 1$ in Eq. 22. Eqs. 20 and 21 are combined to yield a predictive expression for the new field

$$\bar{E}'_j = \left(\bar{I} + \sum_i z_i \bar{u}_i \Delta \bar{C}_{i,j}\right) \Big/ \sum_i z_i^2 \bar{u}_i \bar{C}_{i,j}, \tag{23}$$

which is the starting equation for the iterative procedure since the result is inserted into Eq. 20 to solve for fluxes. Eq. 11 may be rewritten using these flux values

$$\bar{C}'_{i,j} = \bar{C}_{i,j} - (\bar{J}_{i,j+1} - \bar{J}_{i,j}), \tag{24}$$

where $\bar{C}'_{i,j}$ is a new concentration due to transport during a subsequent time interval.

At this point, the equilibrium Eq. 2 is applied in each volume element using

$$\bar{C}^*_{X,j} = \bar{C}_{X,j} + \bar{C}_{MX,j}, \tag{25}$$

and the reduced forms of Eqs. 2 and 3

$$\bar{C}_{M,j} + \bar{C}_{N,j} = \bar{C}_{X,j}, \tag{26}$$

$$\bar{K}_f = \bar{C}_{MX,j}/(\bar{C}_{M,j})(\bar{C}_{X,j}) = K_f C_o, \tag{27}$$

$\bar{C}^*_{X,j}$ and $\bar{C}_{N,j}$ are known and constant during this step. The new concentration of X^-, $\bar{C}'_{X,j}$, which satisfies the equilibrium obeys a quadratic of one variable

$$\bar{K}_f(\bar{C}'_{X,j})^2 - \bar{K}_f \bar{C}'_{X,j} \bar{C}_{N,j} + \bar{C}'_{X,j} - \bar{C}^*_{X,j} = 0, \tag{28}$$

and is found by a root search method which maintains high accuracy in the simulation. The results, reinserted into Eqs. 25 and 26, yields other equilibrium concentrations

which are then returned to Eq. 23 where the iterative procedure is started again for a new time interval. The process is continued until a steady state is reached.

The potential at any time is computed from

$$\bar{V} = \ln(a'_M \bar{C}_{M,NVE}/a''_M \bar{C}_{M,1}) - \sum_j \bar{E}_j, \tag{29}$$

where the first term combines the interfacial potentials and the second term corresponds to a trapezoid-rule integration of the fields to yield the diffusion potential. The partition coefficients k_M and k_N are assumed to be 1 to simplify the procedure. For high mobility values, such as those used for most of these simulations, the first values (at $\bar{t} = 1$) have a rather large error. Not until $\bar{t} = 10$ does the time response converge with accurate values extrapolated from simulations utilizing lowered mobilities.

CHECKS ON THE SIMULATION

There were numerous checks on the accuracy and authenticity of the results. Primarily, convergence of the various computed values and attainment of a steady state in the diffusion time of the membrane were used as gross checks on the simulation. Accuracy of some simulated values was checked by comparison with calculated, closed-form expressions for steady-state concentration profiles, diffusion potentials, and overall membrane potential values. Finally, there were internal checks such as maintainance of electroneutrality, conservation of mass of the sites within the membrane, compliance with chemical equilibrium laws, and compliance with a generally valid, space-independent, steady-state combination of concentrations. From the total flux Eqs. 30 A–C, the steady-state condition $J_X^* = 0$ and electroneutrality.

$$J_X^*/u_X = -RT(\partial C_X/\partial x) - C_X FE - RT(u_{MX}/u_X)(\partial C_{MX}/\partial x), \tag{30 A}$$

$$J_M^*/u_M = -RT(\partial C_M/\partial x) + C_M FE - RT(u_{MX}/u_M)(\partial C_{MX}/\partial x), \tag{30 B}$$

$$J_N^*/u_N = -RT(\partial C_N/\partial x) + C_N FE, \tag{30 C}$$

one finds

$$\frac{J_M^*}{u_M} + \frac{J_N^*}{u_N} = -2RT\frac{\partial C_X}{\partial x} - RT\frac{\partial C_{MX}}{\partial x}u_{MX}\frac{(u_M + u_X)}{(u_M u_X)} = \text{constant}. \tag{30 D}$$

Therefore

$$2C_X + u_{MX}[(u_M + u_X)/u_M u_X]C_{MX} = \text{linear function of distance}. \tag{31}$$

This expression was used to check the simulation at zero current in the steady state.

RESULTS

Specification of System Parameters Used to Illustrate Simulations

The various cases simulated may be totally described by the following reduced input parameters: $\bar{C}_X^*$, total site concentration; $\bar{u}_i$, mobilities; (z_i), charge on the ions; (NVE),

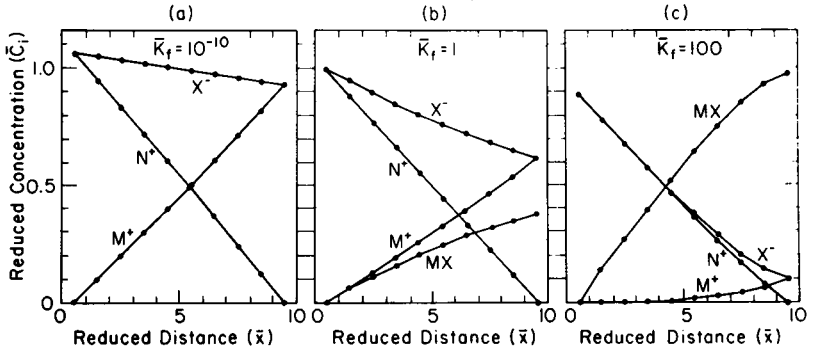

FIGURE 3 Steady-state concentration profiles for a liquid ion exchanger membrane containing permeable cation M^+ and N^+ and trapped sites X^-. $C_X^* = 1.0, \bar{u}_X = 0.20\ \bar{u}_M = 0.45, \bar{u}_N = 0.35, \bar{u}_{MX} = 0.20$. Outside bathing activities: $a'_M = 10^{-10}$, $a'_N = 10^{-4}$, $a''_M = 1$, $a''_N = 10^{-10}$. Left: $\bar{K}_f = 10^{-10}$. Middle: $\bar{K}_f = 1$. Right: $\bar{K}_f = 100$.

number of volume elements; $\bar{K}_f$, ion pair formation constant for M^+; a'_M, a'_N, activities of cations on the left side of the membrane; (a''_M, a''_N), activities of cations on the right side of the membrane; (k_M, k_N), single-ion partition coefficients; $\bar{I}$, current.

Parameters in parentheses are those which cannot be varied (z_i) and those for which there is little reason for variance (k_i, a''_i, NVE). Values used for all simulations reported in this paper are: $z_i = +1$ for M, N; -1 for X; 0 for MX; $k_i = 1$ for M and N; $a''_M = 1$; $a''_N = 10^{-10}$; NVE = 10. Thus, there are only six basic parameters which are to be varied: $\bar{u}_i$, $\bar{C}_X^*$, a'_M, a'_N, $\bar{K}_f$, and $\bar{I}$. The fundamental results obtained from the simulations are: $\bar{C}_i$, concentrations as a function of time, distance, and input parameters; $\bar{V}$, potential as a function of time, distance, and input parameters; $\bar{E}_j$, fields as a function of time, distance, and input parameters. Two general cases have been studied: (*a*) $a'_N/a'_M \ll 1$, i.e. a single (M^+) cation membrane; (*b*) $a'_N/a'_M \gg 1$, membrane with N^+ on left hand and M^+ on the right.

Zero Current Steady-State Responses

$a'_N/a'_M \ll 1$. In the single cation-containing membrane system, all concentration profiles through a membrane are constant ("flat") and independent of the external bathing solution activities. With no ion association, $\bar{C}_X = \bar{C}_M = \bar{C}_X^*$ and $\bar{C}_N = \bar{C}_{MX} = 0$. Ion-pairing merely raises or lowers $\bar{C}_X$ and $\bar{C}_M$ to common values $\bar{C} = [-1 + (1 + 4\bar{K}_f\bar{C}_X^*)^{1/2}]/2\bar{K}_f$ and $\bar{C}_{MX} = \bar{C}_X^* - \bar{C}$. Profiles are independent of time after an ion activity step on either side because charging of the geometrical capacitance of the membrane does not appear in this level of simulation. Similarly, the potential of the membrane is $\bar{V} = \ln(a'_M/a''_M)$ at all times. All electric intensities inside the membrane are zero and the potential is totally determined by external activities outside each interface. However, voltage profiles do vary with $\bar{K}_f$ as internal concentrations vary, as shown in Fig. 2.

$a'_N/a'_M \gg 1$. With no ion-pairing, site profiles are linear (Fig. 3, left), but individual ion profiles differ from linearity. Because $\bar{u}_M = 0.45$, $\bar{u}_N = 0.35$, $\bar{C}_N$

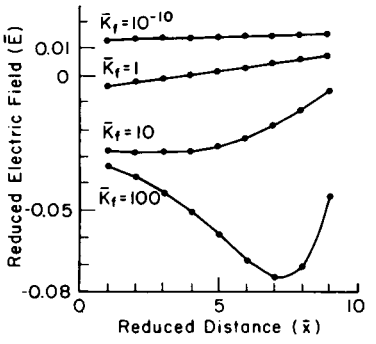

FIGURE 4

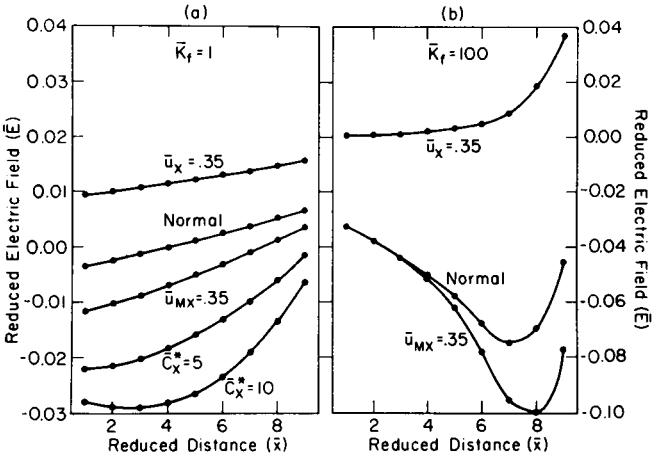

FIGURE 5

FIGURE 4 Steady-state field profiles in the interference region for a cation permselective liquid ion exchanger membrane bathed in $a''_M = 1$ on right (reference side) and $a'_N = 10^{-4}$, $a'_M = 10^{-10}$ on the left; mobilities are $\bar{u}_M = 0.35$, $\bar{u}_N = 0.35$, $\bar{u}_{MX} = 0.20$, $\bar{u}_X = 0.20$, and $\bar{C}_X^* = 1.0$. $\bar{K}_f$ values are varied.

FIGURE 5 Effects of site concentration and mobilities on steady-state field profiles in the interference region for mild association $\bar{K}_f = 1$ and strong association $\bar{K}_f = 100$. The cation permselective liquid ion exchanger membrane is bathed in $a''_M = 1$ on right (reference side) and $a'_N = 10^{-4}$, $a'_M = 10^{-10}$. Mobilities are $\bar{u}_M = 0.45$, $\bar{u}_N = 0.35$ unless otherwise noted, $\bar{u}_X = 0.2$, $\bar{u}_{MX} = 0.2$, $\bar{C}_X^* = 1$; "Normal" curves: (*a*) $\bar{K}_f = 1$, (*b*) $\bar{K}_f = 100$.

is slightly concave downward while $\bar{C}_M$ is concave upward. The site profile, $\bar{C}_X$, is tipped in response to $\bar{u}_X$, $\bar{u}_M$, and $\bar{u}_N$. Only in the special case that $\bar{u}_N = \bar{u}_M$, is $\bar{C}_X$ flat and the concentration profiles of the cations linear. Varying $\bar{C}_X^*$ causes proportional variations in the counterion profiles. The mobility of the site, $\bar{u}_X$, has no effect on profiles in the steady state. These steady-state results for $\bar{K}_f = 0$ agree with the theoretical equations by Conti and Eisenman (4).

Increasing ion association produces concentration profiles that deviate strongly from linearity, as shown in the middle and right of Fig. 3, and mobilities of all species affect the profiles. Increasing $\bar{u}_{MX}$ steepens the site profile while increasing $\bar{u}_X$ has the opposite effect (for $\bar{u}_M > \bar{u}_N$). Consideration of the middle and right figures shows that increasing $\bar{K}_f$ causes greater tipping and further deviations from linearity in the site profile, $\bar{C}_X$.

Electric fields for the completely dissociated case with $\bar{u}_M > \bar{u}_N$ are positive and nearly constant across the membrane. Decreasing $\bar{u}_M/\bar{u}_N$ decreases the field values from positive to negative as $\bar{u}_N$ becomes greater than $\bar{u}_M$. $\bar{C}_X^*$, $\bar{u}_X$, and $\bar{u}_{MX}$ have no effect. With increasing ion-pairing, the fields become negative, as illustrated in Fig. 4. Only fields in the interference region are illustrated. A great deal of curvature is introduced at $\bar{K}_f \approx 10$ on the right side of the membrane where there is marked curvature of the concentration profiles and maximum complex formation. In Fig. 5*a* and 5*b*,

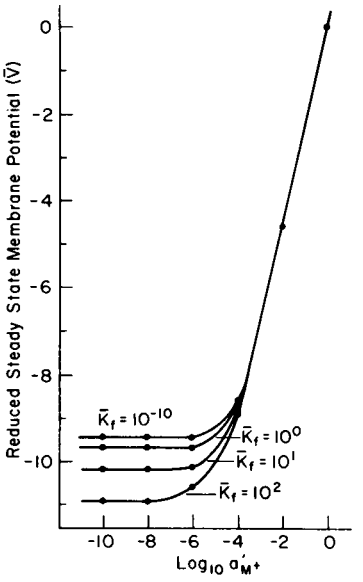

FIGURE 6

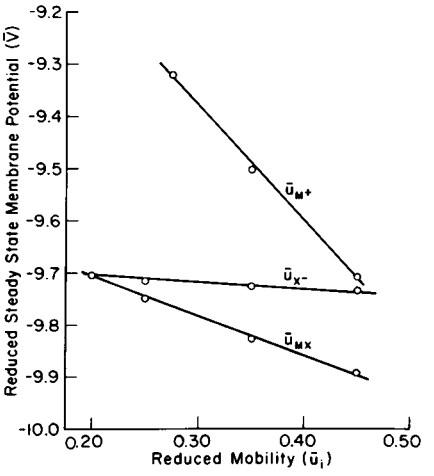

FIGURE 7

FIGURE 6 Computed steady-state membrane potential responses for a cation permselective liquid ion exchanger membrane bathed in $a''_M = 1$, $a''_N = 10^{-10}$ on right (reference side) and $a'_N = 10^{-4}$ on left with varying a'_M. Interference region response dependence on $\bar{K}_f$ is illustrated. $\bar{u}_M = 0.45$, $\bar{u}_N = 0.35$, $\bar{u}_X = 0.20$, $\bar{u}_{MX} = 0.20$, $\bar{C}^*_X = 1.0$ for all curves.

FIGURE 7 Computed steady-state membrane potentials in the interference region for a cation permselective liquid ion exchanger membrane bathed in $a''_M = 1$ and $a''_N = 10^{-10}$ on right (reference side) and $a'_N = 10^{-4}$ on left with $a'_M \ll a'_N$. Mobility of an individual species is varied while holding others constant at: $\bar{u}_M = 0.45$, $\bar{u}_N = 0.35$, $\bar{u}_{MX} = 0.20$, $\bar{u}_X = 0.20$; $\bar{K}_f = 1$.

field variations due to changes in $\bar{C}^*_X$ and ion mobilities for associated membranes in the interference region are shown. Increasing $\bar{C}^*_X$ causes a negative field and curvature similar to those which arise when $\bar{K}_f$ is increased. Increases in $\bar{u}_X$ at intermediate and high degrees of ion-pairing cause a positive field shift and affect the curvature of the fields similar to a decrease in $\bar{K}_f$. Increasing $\bar{u}_{MX}$ produces the opposite effect.

The membrane potential for the completely dissociated case in the steady state is

$$\bar{V} = \ln[(a'_M + K^{pot}_{M,N} a'_N)/a''_M], \tag{32}$$

where $K^{pot}_{M,N} = K_{iexch}\bar{u}_N/\bar{u}_M$, $a''_N = 0$, and $\bar{V}$ is independent of the total site concentration $\bar{C}^*_X$. Simulated steady-state potentials are given in Fig. 6 for a typical situation where the interference a'_N is 10^{-4} M, and a'_M is varied from 10^{-10} to 1 M. The expected interference potential occurs for $a'_M \ll a'_N$. In the absence of ion association, computed $K^{pot}_{M,N}$ has the theoretical value. An increase in ion association between X^- and M^+ affects the potential response (a negative shift) only in the interference potential region. This result means that association favors M^+ in the membrane and reduces the effective interference by N^+. The shift in potential is primarily due to the decrease

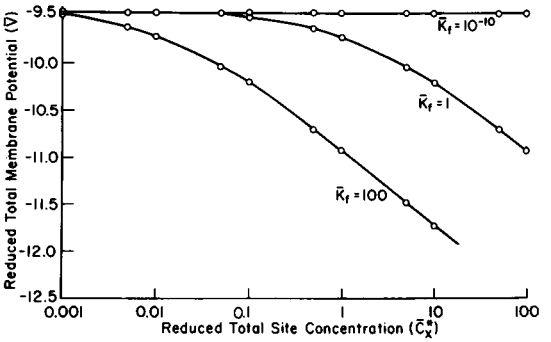

FIGURE 8

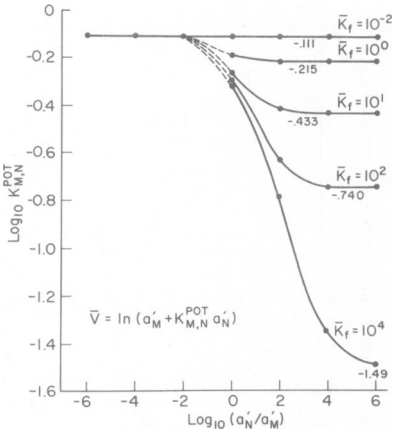

FIGURE 9

FIGURE 8 Dependence of membrane potential on total site concentration for dissociated and associated membrane. Intereference responses are considered: $a_N' = 10^{-4}$, $a_M'' = 1$, $a_M' = 10^{-10}$ $a_N'' = 10^{-10}$. $\bar{u}_N = 0.35$, $\bar{u}_M = 0.45$, $\bar{u}_{MX} = 0.20$, $\bar{u}_X = 0.20$. K_f values are indicated next to each curve.

FIGURE 9 Potentiometric selectivity coefficients for a cation permselective liquid ion exchanger membrane bathed in $a_M'' = 1$ on right (reference side) with variation of a_N'/a_M'. Mobilities are $\bar{u}_M = 0.45$, $\bar{u}_N = 0.35$, $\bar{u}_{MX} = 0.20$, $\bar{u}_X = 0.20$. Total site concentration $\bar{C}_X^* = 1.0$. Note that responses are independent of absolute values of a_N' and a_M'.

in $\bar{C}_M(d)$. A change in the mobilities of any of the four species also affects selectivity which changes the interference potential, as can be seen in Fig. 7. Slopes for the dependence of potential on mobilities are unfortunately not constant but depend on the value of the formation constant, $\bar{K}_f$, as shall be discussed in more detail below.

Direct calculation of $K_{M,N}^{pot}$ for systems involving ion association is algebraically complicated and has not been attempted. However, there are levels of approximation from which some dependencies on mobilities and $\bar{K}_f$ can be isolated. For example, in the interference region with $a_M'' = 1$, $a_N' \gg a_M'$, assuming linear species profiles and constant $\bar{C}_X^*$ everywhere in the membrane.

$$K_{M,N}^{pot} \approx K_{iexch}(u_N/u_M)[(u_N/u_M)(K_f\bar{C}_X^*)^{1/2}]^{-u_{MX}/u_N}, \tag{33}$$

where $K_{iexch} = k_N/k_m = 1$ and $K_f\bar{C}_X^* > 1$. In a higher level approximation accounting for the tipping of $\bar{C}_X^*$, an inverse dependence of $K_{M,N}^{pot}$ on u_X is anticipated. Simulated results are in directional agreement with simplified theory. Furthermore, membranes with equal products ($\bar{K}_f \cdot \bar{C}_X^*$) exhibit equal interference potentials (Fig. 8), as this simple approximation suggests. When $\bar{C}_X^*$ is increased the interference potential again moves negatively, which is understood by observing the concentration changes produced. It is found that $\bar{C}_M(0)$ roughly increases as $\bar{C}_X^*$ while $\bar{C}_M(d)$ increases as $(\bar{C}_X^*)^{1/2}$, thus producing a negative shift. Flattening or steepening of the $\bar{C}_X$ concentration profile with changes in the various mobilities also contributes to the resulting interference potential shifts.

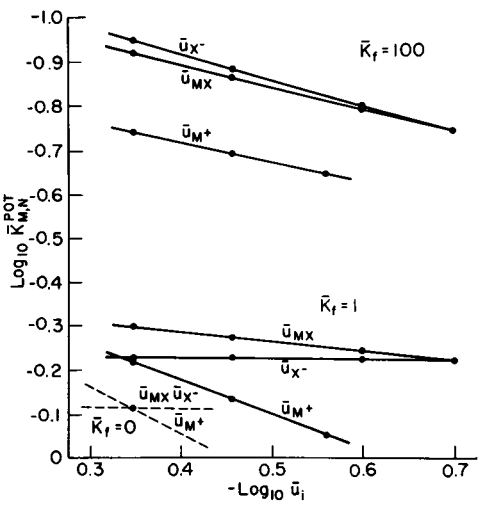

FIGURE 10

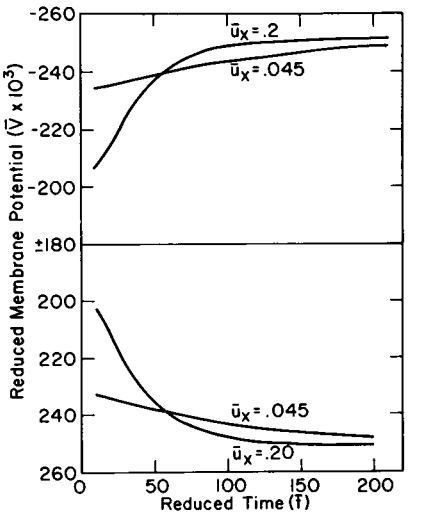

FIGURE 11

FIGURE 10 Variation of potentiometric selectivity coefficients with mobilities of membrane species for zero, intermediate, and strong association. Conditions are the same as in Fig. 7.

FIGURE 11 Low frequency or long time constant responses of a liquid ion exchanger membrane electrode to step activity changes. The effect of varying site mobility, $\bar{u}_X$, on shape of transient potential vs. time response for a completely dissociated membrane. $\bar{C}_X^* = 1$, $a''_M = 1$, a'_N stepped from 0 to 1, a'_M stepped from 1 to 10^{-10}. Top curve: $\bar{u}_M = 0.35$, $\bar{u}_N = 0.45$. Bottom: $\bar{u}_M = 0.45$, $\bar{u}_N = 0.35$.

The apparent potentiometric selectivity coefficient, $K^{pot}_{M,N}$ can be calculated from the expression

$$K^{pot}_{M,N} = [\exp(\bar{V}) - a'_M]/a'_N. \tag{34}$$

This value is equal to $K_{iexch}(\bar{u}_N/\bar{u}_M)$ for a completely dissociated membrane in the steady state, but becomes smaller for an increase in $\bar{K}_f$, as shown in Fig. 9. This result was predicted in Eq. 33. The simulations were performed for various ratios of a'_N/a'_M, while varying the absolute value of a'_N. Buck (16) had previously predicted for reversible membranes with permselective ions of the same charge that potentiometric selectivity coefficients should depend only on activity ratios and not on absolute activity values. When ion association exists, $K^{pot}_{M,N}$ becomes dependent (inversely) on the value of $\bar{u}_X$, $\bar{u}_{MX}$, $\bar{u}_M$, and $\bar{C}_X^*$. There is an increase in $K^{pot}_{M,N}$, of course, for an increase in $\bar{u}_N$. These latter results are illustrated in Fig. 10. In the limit $\bar{u}_X = 0$ (not shown), selectivity decreases to the nonassociated value.

Transient Responses to Ion Activity Steps on One Side

Total-potential transient responses to an "ion activity step" on the left side of membrane ($a'_N/a'_M \ll 1$ with $a'_M = 1$ to $a'_N/a'_M \gg 1$ with $a'_N = 1$) show a remarkable variation with the extent of ion-pairing. With no complexation, positive or negative-going

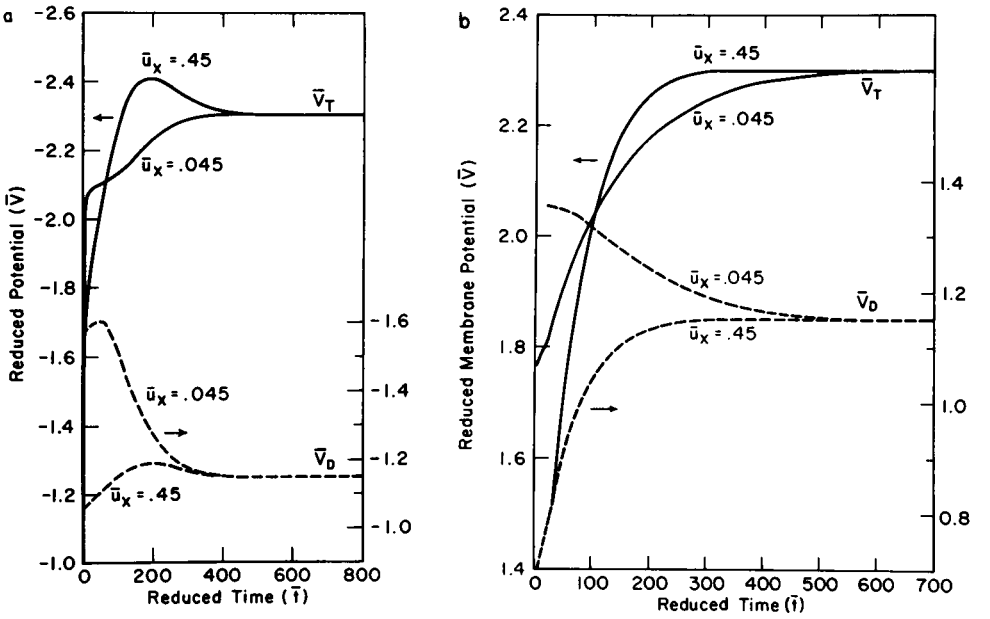

FIGURE 12 Low frequency or long time constant responses of a liquid ion exchanger membrane electrode to step activity changes with large cation mobility differences. $K_f = 10^{-10.}$ External activities same as in Fig. 11. $\bar{C}_X = 1.$, (*a*) $\bar{u}_M = 0.45$, $\bar{u}_N = 0.045$, $\bar{u}_X$ indicated next to curves. Upper curve is total potential response. Lower curve is diffusional component response. (*b*) $\bar{u}_M = 0.045$, $\bar{u}_N = 0.45$, $\bar{u}_X$ indicated next to curves. Upper curve is total potential, lower curve is diffusional component.

monotonic transients are expected depending on whether $K^{pot}_{M,N}$ is greater or less than unity, respectively. Since the simulation does not cover short-time double-layer charging effects, the high frequency (short-time) exponential response with a time constant given by the product of membrane high frequency resistance and geometric capacitance is not seen. The so-called low frequency or long-time response occurs by massive readjustment of the interior concentrations and is thus expected to show Warburg character, e.g. a diffusion-migration time constant depending on the square of the membrane thickness divided by a net diffusion coefficient due to coupling of the ions' motions. Clearly, the net diffusion coefficient depends on the mobilities of all the ions, as is illustrated in Fig. 11.

However, monotonic transient response is not universally observed, even for these passive systems. The primary factor needed to produce an observable "overshoot" in potential-time response is low mobility of the entering ion, N^+, relative to the mobility of the ion already in the membrane, M^+. At the same time, the site mobility must be about the same as that of the exiting ion. A third type of behavior also occurs, which is reminiscent of two time constants. These cases are illustrated in Fig. 12*a*. Note, however, that low mobility of the exiting ion and high mobility of the entering ion do not produce the same effect. Response for the latter case is shown in Fig. 12*b*. In both

Fig. 12*a* and *b*, the total potential as well as the diffusion component are illustrated. It is well known that total steady-state membrane potentials are exactly twice the steady-state diffusion components (17).

Transient responses to step ion activity changes for associated membranes are still more complicated. Using the conditions as above, e.g. using mobilities $\bar{u}_X = 0.2$, $\bar{u}_M = 0.45$, $\bar{u}_N = 0.35$, and $\bar{u}_{MX} = 0.2$, transient responses are quite different in magnitude and direction for $\bar{K}_f = 0$, $\bar{K}_f = 1$, and $\bar{K}_f = 100$. In each of these, the final steady-state response is also different. These three transients are illustrated in Fig. 13. The initial condition in each case is a membrane bathed by symmetrical solutions; $a''_M = a'_M = 1$, $a'_N = a''_N = 10^{-10}$, and therefore $\bar{V} = 0$. The ion activity step excitation on the left side of the membrane raises a'_N to 10^{-4} and lowers a'_M to 10^{-10}, a step which will produce a negative steady-state potential for the K_{iexch} and $\bar{u}_N/\bar{u}_M$ ratios which have been considered. The response for a dissociated membrane is, as mentioned, a monotonic downward transient. For a highly associated membrane, the response to the initial extraction is more negative and the transient is in the opposite direction and is no longer monotonic. Experimental time responses similar to this have been observed by Reinsfelder and Schultz (18). At an intermediate degree of complexation, $\bar{K}_f = 1$, the response is initially downward, dropping past the steady-state potential, and then reversing direction and slowly climbing back to the final value. The extent of the transient is different for these cases.

Potential changes after the initial extraction may be overlooked when considering

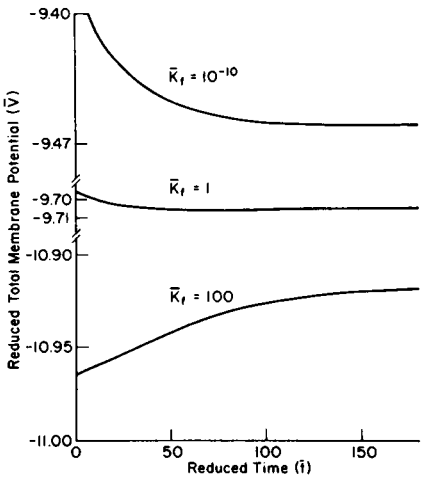

FIGURE 13

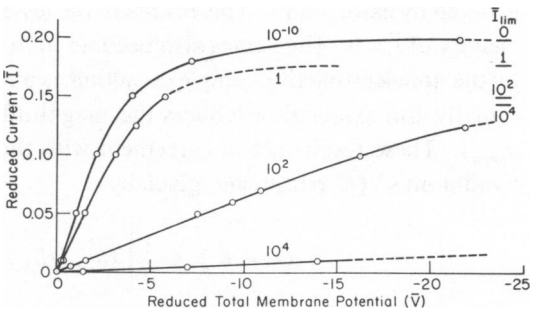

FIGURE 14

FIGURE 13 Low frequency responses to step activity changes at differing degrees of ion association. $\bar{C}^*_t = 1$, $\bar{u}_M = 0.45$, $\bar{u}_N = 0.35$, $\bar{u}_x = 0.20$, $\bar{u}_{MX} = 0.20$. $a''_M = 1$, a'_M stepped from 1 to 10^{-10}, a'_N stepped from 0 to 10^{-4}. $\bar{K}_f$ is indicated next to each curve.

FIGURE 14 Steady-state current-voltage curves for liquid ion-exchange membrane electrodes at various degrees of ion-pairing, single cation case. $a'_M = a''_M = 1$. $\bar{C}^*_t = 1$, $\bar{u}_M = 0.45$, $\bar{u}_X = 0.2$, $\bar{u}_{MX} = 0.2$. K_f values indicated next to curves.

the effects of ion association. However, variations in the size and shape of the transients occur for variations in the mobilities of the species, as well as the degree of ion association. This fact complicates the ability to extract information about complex formation from "ion-step" transient data.

Steady-State Current-Voltage Curves

$a'_N/a''_M \ll 1$, $a'_M = 1$. Current-voltage characteristics of nonassociated membranes with symmetrical single-salt bathing solutions have been described by Conti and Eisenman (4). Their treatment has been extended to include membranes with ion association by Sandblom et al. (7). Current-voltage curves for various degrees of ion association are simulated and the results compared with the treatment of Sandblom.

For the nonassociated case, passage of current produces a tipping of the $\bar{C}(= \bar{C}_x = \bar{C}_M)$ concentration profile until the concentration at the existing side of the membrane (d, for positive $\bar{I}$) reaches zero. The current at which this occurs is the limiting current, and agrees with values calculated from known, closed-form expressions for limiting currents of dissociated liquid membranes. Likewise, the shape of the curve, shown in Fig. 14, is a tanh function whose values agree with those calculated from the current-voltage equations of Conti and Eisenman (4), and Buck (17).

In highly associated membranes, the concentrations of the ionic species are lower, and yet, a small current will not produce a significant skewing of concentrations, because of the "reservoir" effect, until very high field strengths are reached. At this point, the ionic and ion-pair concentrations become zero at the exiting side and the limiting current is reached. For our case, in which the reduced ionic mobility, defined as

$$\bar{u}_{\text{ionic}} = 2[\bar{u}_M \bar{u}_X/(\bar{u}_M + \bar{u}_X)], \tag{35}$$

is greater than the complex mobility, $\bar{u}_{MX}$, the net coupled membrane ion mobility is lowered by association. This results in the lessening of the slope of the $\bar{I}$-$\bar{V}$ curve in the vicinity of $\bar{I} = 0$. The curves also become more linear with association, a result caused by the nonelectroactive complexes acting as a reservoir for the dissociated ions. Additionally, ion association reduces the magnitude of the limiting current (when $\bar{u}_{MX} < \bar{u}_{\text{ionic}}$). These results are in agreement with those predicted by Sandblom's treatment. Sandblom's "$\bar{Q}$" parameter, given by

$$\bar{Q} = \bar{C}_X^* + \frac{1}{d}\left[(\bar{u}_{\text{ionic}}/\bar{u}_{MX}) - 1\right]\int_0^d \bar{C}_X \, dx, \tag{36}$$

is evaluated by integrating the site profile, $\bar{C}_X$, which resulted from the simulation. The $\bar{Q}$ values were found to be nearly invariant with $\bar{I}$, even for intermediate degrees of association, since our $\bar{u}_{\text{ionic}}$ and $\bar{u}_{MX}$ values were nearly equal. These Q values were used to evaluate Sandblom's expression for the limiting current, which are the resultant values from the current-voltage curves of the simulation for lower values of $\bar{K}_f$. However, the simulation is not able to reach the theoretical limiting current for higher degrees of ion association. $\bar{Q}$ values are inserted into Sandblom's expression for

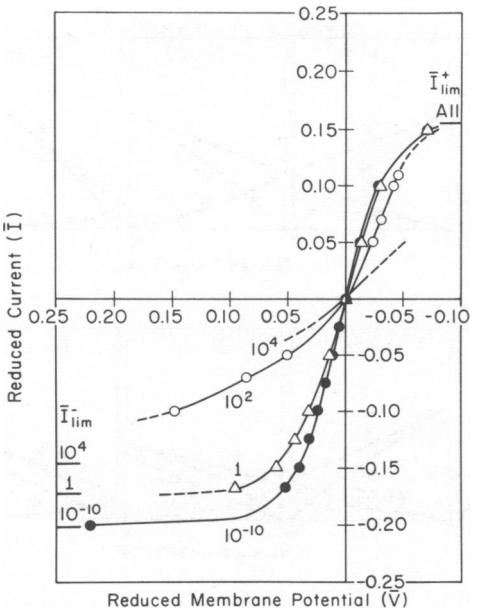

FIGURE 15 Steady-state current-voltage curves for liquid ion-exchange membrane electrode at various degrees of ion-pairing. $C^*_X = 1$, $\bar{u}_M = 0.45$, $\bar{u}_N = 0.35$, $\bar{u}_X = 0.2$, $\bar{u}_{MX} = 0.2$. Bathing solutions: $a'_M = 1, a'_M = 10^{-10}$, $a'_N = 10^{-4}$. $\bar{V} = \bar{V}_{obs} - \bar{V}_o$, where $\bar{V}_o$ is the potential at $\bar{I} = 0$. $\bar{K}_f$ values are indicated next to each curve. $\bar{I}_{lim}$ computed from Sandblom is indicated.

the various points on the current-voltage curves and agreement is found with points given by the simulation.

$a'_N/a'_M \gg 1, a'_N = 1$. Current-voltage curves in the interference region are shown in Fig. 15. The curve for the completely dissociated case is seen to possess different shapes for positive or negative currents. The concentration profiles' change with current is shown in Fig. 16*a*. As positive current is passed, N^+ is swept into the membrane from the left. The site profile, $\bar{C}_X$, is tipped more steeply as current is increased, but remains linear. A steepening of the N^+ profile can be observed which becomes more curved downward as current increases. Likewise, the concentration of M^+ decreases for positive current; the profile becomes more curved upward. At the limiting current, N^+ is the only cation in the membrane and its concentration profile, which is high on the entering side, has dropped to zero at the right interface. Thus, the limiting current is dependent on the mobility of N^+ only, and is given by

$$\bar{I}^+_{lim} = 4\bar{u}_N \bar{C}^*_X/(\text{NVE} - 1). \tag{37}$$

Under negative current conditions, M^+ is swept through the membrane from the right. At some negative current, since $\bar{u}_M > \bar{u}_N$, the mobility difference is completely offset by the current and the membrane interior is now symmetrical with respect to concentrations, i.e. the site profile, $\bar{C}_X$, is flat, and the cation profiles, $\bar{C}_M$, $\bar{C}_N$, are linear. As the current is made more negative, the site profiles show positive slope;

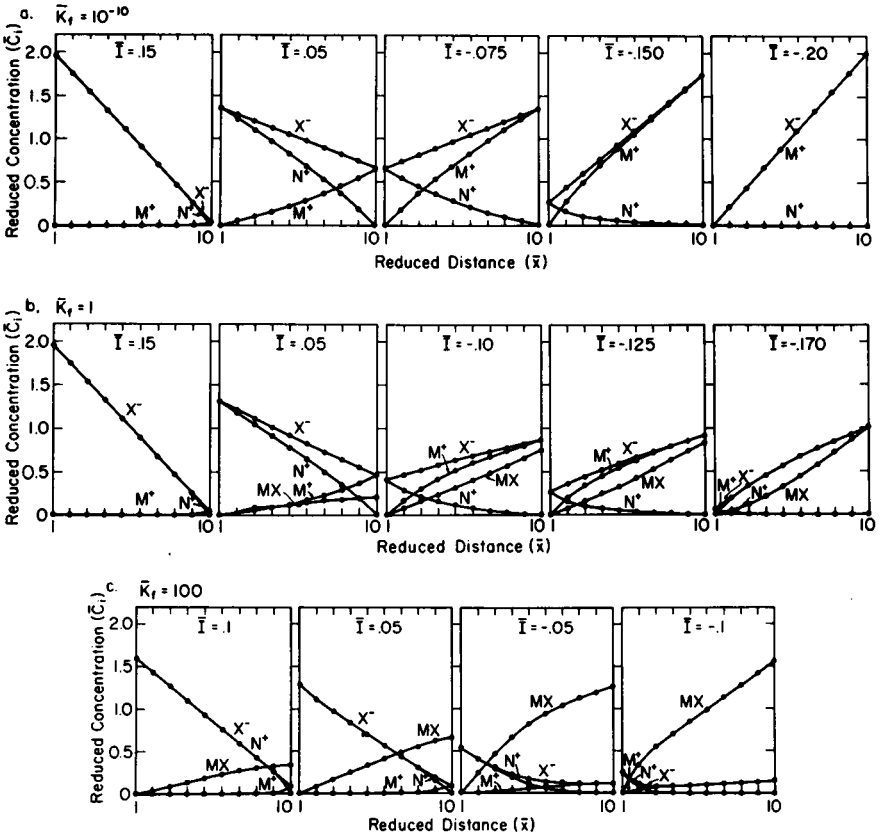

FIGURE 16 Steady-state concentration profiles for various currents and degrees of ion-pairing. Conditions are the same as those for Fig. 15. Current values and $\bar{K}_f$ values are indicated in each.

$\bar{C}_M$ is now curved downward and $\bar{C}_N$ is curved upward. At the limiting current, i.e. when the site concentration at the left interface is zero, M^+ completely fills the membrane. The negative limiting current is solely dependent on $\bar{u}_M$. Thus the current-voltage curve is partially rectified, i.e. the negative and positive limiting currents differ since $\bar{u}_N \neq \bar{u}_M$. The nonassociated curve is in agreement with that calculated from the equations of Conti and Eisenman (4).

Ion-pairing affects the current-voltage curves in different ways, depending on whether positive of negative current is passed, as was seen in Fig. 15. Fig. 16*b* and *c* illustrate the changes in the concentration profile for $\bar{K}_f = 1$ and $\bar{K}_f = 100$. With the passage of positive current, N^+ enters the membrane and $\bar{C}_X$ is tipped, as occurred in the dissociated case. However, there is a significant amount of complex, MX, present, and since its mobility, $\bar{u}_{MX}$, is less than $\bar{u}_{\text{ionic}}$ (computed from Eq. 35, using $\bar{u}_M$ or $\bar{u}_N$), the slope of the current-voltage curve is reduced for increasing complexation. The concentrations, $\bar{C}_M$ and $\bar{C}_{MX}$ are lowered with the passage of positive current as

M^+ is pushed out of the membrane and MX dissociates concurrently. At the limiting current, all of MX has dissociated and M^+ has been swept out of the membrane, and thus the concentration profiles are identical for all degrees of ion-pairing at the positive limiting current. Obviously, the positive limiting current is independent of ion-pairing, but the current-voltage curves are less steep and more nearly linear for associated membranes up to the limiting current.

The negative current-voltage curves look very similar to those for membranes containing only M^+. However, since there is some N^+ in the membrane until the limiting current is reached, the curves are not identical. As N^+ is pushed from the membrane, $\bar{C}_{MX}$ increases, the membrane resistance changes, and therefore the curves display less linearity than in the single-ion case. At the limiting currents, there is no more N^+ present and the concentration profiles are identical to those of single (M^+) cation membranes. Thus, negative limiting currents are equal to those of the single-cation membrane for equal degrees of ion association.

It can be seen that increased linearity of the current-voltage curves is a distinguishing feature of associated membranes. As can also be seen from the $\bar{K}_f = 1$ and $\bar{K}_f = 100$ curves of Fig. 15, a sharper transition near the limiting current occurs when a less complexing ion is swept through a membrane. In addition, less linearity is seen when the more complexing ion is swept through, in comparison with the single-cation case. However, limiting current concentration profiles, and therefore the value of the limiting currents, are seen to be identical with those of the single-cation case, given the same degree of association.

This study was supported by National Science Foundation Grant No. MPS-7500970.

Received for publication 18 December 1975.

REFERENCES

1. TOREN, E. C., JR., and R. P. BUCK. 1970. Potentiometric titrations. *Anal. Chem.* **42**:284R.
2. BUCK, R. P. 1972. Ion selective electrodes, potentiometry, and potentiometric titrations. *Anal. Chem.* **44**:270R.
3. BUCK, R. P. 1974. Ion selective electrodes, potentiometry, and potentiometric titrations. *Anal. Chem.* **46**:28R.
4. CONTI, F., and G. EISENMAN. 1966. The steady state properties of an ion exchange membrane with mobile sites. *Biophys. J.* **6**:227.
5. SANDBLOM, J., G. EISENMAN, and J. L. WALKER, JR. 1967. Electrical phenomena associated with the transport of ions and ion-pairs in liquid ion-exchange membranes. I. Zero current properties. *J. Phys. Chem.* **71**:3862.
6. SANDBLOM, J., G. EISENMAN, and J. L. WALKER, JR. 1967. Electrical phenomena associated with the transport of ions and ion-pairs in liquid ion-exchange membranes. II. Nonzero current properties. *J. Phys. Chem.* **71**:3871.
7. SANDBLOM, J. 1969. Liquid ion-exchange membranes with weakly ionized groups. I. A theoretical study of their steady state properties. *J. Phys. Chem.* **73**:249.
8. BUCK, R. P., and J. R. SANDIFER. 1973. Mixed divalent, univalent cation responses of completely ionized liquid membrane systems. *J. Phys. Chem.* **77**:2122.
9. MACDONALD, J. R. 1974. Binary electrolyte small-signal frequency response. *J. Electroanal. Chem. Interfacial Electrochem.* **49**:161.

10. MACDONALD, J. R. 1974. Simplified impedance/frequency-response results for intrinsically conducting solids and liquids. *J. Chem. Phys.* **61**:3977.
11. FELDBERG, S. W. 1969. Digital simulation: a general method for solving electrochemical diffusion-kinetic problems. *In* Electroanalytical Chemistry. Vol. 3. A. J. Bard, editor. Marcel Dekker, New York.
12. SANDIFER, J. R., and R. P. BUCK. 1974. Improvements in digital simulations. *J. Electroanal. Chem. Interfacial Electrochem.* **49**:161.
13. COHEN, H., and S. W. COOLEY. 1965. The numerical solution of the time-dependent Nernst-Planck equations. *Biophys. J.* **5**:145.
14. SANDIFER, J. R., and R. P. BUCK. 1975. An algorithm for simulation of transient and alternating current electrical properties of conducting membranes, junctions, and one-dimensional, finite galvanic cells. *J. Phys. Chem.* **79**:384.
15. EISENMAN, G. 1969. Theory of membrane electrode potentials: An examination of the parameters determining the selectivity of solid and liquid ion-exchangers and of neutral ion-sequestering molecules. *In* National Bureau of Standards Special Publication #314. R. Durst, editor. U.S. Government Printing Office, Washington, D.C.
16. BUCK, R. P. 1974. Reporting concentration- and concentration ratio-dependent selectivity coefficients for ion selective electrodes. *Anal. Chim. Acta.* **73**:321.
17. BUCK, R. P. 1973. Steady state space charge effects in symmetric cells with concentration polarized electrodes. *J. Electroanal. Chem. Interf. Electrochem.* **46**:1.
18. REINSFELDER, R. E., and F. A. SCHULTZ. 1973. Anion selectivity studies on liquid membrane electrodes. *Anal. Chim. Acta.* **65**:425.